Heat stress in tropical highland regions: the case of Kenya during February 2024

G. Chagnaud[1], J. Gacheru[2], C. M. Taylor[1,3] and C. E. Birch[4]

[1] *UK Centre for Ecology and Hydrology, Wallingford, UK*
[2] *Kenya Meteorological Department, Nairobi, Kenya*
[3] *National Centre for Earth Observation, Wallingford, UK*
[4] *School of Earth and Environment, University of Leeds, Leeds, UK*

Introduction

Heatwaves, which can cause episodes of high heat stress, are considered 'silent killers' for two interrelated reasons: first, unlike other extreme weather events such as hurricanes or floods, they can often leave no physical trace of their passage; second, the effects of heat stress on the human body can build gradually and have serious consequences including death. These effects often add to pre-existing health conditions, so people in vulnerable groups (older, pregnant, those with chronic illnesses, etc.) are affected more (Luber and McGeehin, 2008; Ebi *et al*., 2021; Nunes, 2024).

Extreme heat events are among the deadliest weather events; climate change has increased heat-related mortality across many parts of the world (Vicedo-Cabrera *et al*., 2021) by increasing their frequency, intensity, duration and areal extent (Matthews *et al*., 2025). These trends will continue in the future even with moderate greenhouse gas emissions (Gasparrini *et al*., 2017; Schwingshackl *et al*., 2021). The impacts of heat stress are numerous, including but not limited to the following: increased morbidity and mortality; productivity declines in various economic sectors; increased tensions on water, food, electricity and healthcare. This is especially the case in sub-Saharan Africa, where populations are both exposed, given the tropical climate, and vulnerable, due to low adaptive capacity and a strong dependence of their economy on outdoor activities. Yet, awareness of the heat–impact relationship, required to mitigate heat risks through relevant adaptation strategies, is still lacking there (Harrington and Otto, 2020).

Ambient humidity plays a role in human heat stress through limiting the efficiency of perspiration (e.g. Baldwin *et al*., 2023). Several heat stress metrics have been developed over the years to provide a more health-relevant measure of the effect of heat on humans than temperature alone (Buzan *et al*., 2015; Perkins, 2015). They all include air temperature and humidity, and some also include solar radiation and wind. Temperature (T) and humidity (specific, q) are weighted differently in these metrics, with two consequences: (i) each metric responds differently to a given change in T and q, and (ii) the sensitivity to T and q depends on the thermal regime, that is, where we sit in the $T - q$ space at a given location and time. As a result, extreme humid heat values are reached through different mechanisms depending on the time of year, location, and the metric used (Sherwood, 2018; Buzan and Huber, 2020; Simpson *et al*., 2023; Ivanovich *et al*., 2024). Therefore, understanding the causes and impacts of humid heat extremes is challenging.

Another difficulty stems in the definition of thresholds for which health impacts of humid heat are expected and/or reported. For instance, the wet-bulb temperature (Twb) value of 35°C has long been considered an upper limit to human survivability (Sherwood and Huber, 2010), based solely on thermodynamical considerations. However, physiological studies have reported serious impacts at Twb values above 24–27°C, depending on personal factors such as age and health condition, as well as on exertion and clothing (Vecellio *et al*., 2022). Furthermore, it is not only survivability that matters, but also liveability. In this regard, Vanos *et al*. (2023) found that '*young adults reach a limit in their ability to perform any activity safely*' at relative humidity of 75% and temperatures above 35.5°C (i.e. Twb ≥ 31.5°C at 1000hPa). For the Heat Index (HI), the US national weather services (NWS) has defined the Caution (HI ∈ [27, 32°C]), Extreme Caution ([33, 39°C]), Danger ([40, 51°C]) and Extreme Danger (HI ≥ 52°C) categories, each with its associated effects on the human body.[1] In short, the heat–health relationship is highly multi-dimensional and context-dependent; an array of approaches, from individual-scale physiological experiments to large-scale epidemio-meteorological studies are needed to improve our understanding of this relationship.

Our case study analysis was motivated by national and social media reports of people complaining about unusually high heat during February 2024 in Kenya.[2,3] This was especially the case between 15 and 20 February 2024 in the highlands of Kenya, one of the most densely populated regions in this part of East Africa that also includes the capital of Kenya, Nairobi (Figure 1a).

The seasonal cycle of rainfall in East Africa shows that February precedes the start of the long rainy season (Figure 1b). February is the second warmest month for average temperature and the first in terms of peak daily temperatures; it is also among the driest months (Figure 1b). The highlands have a cooler and drier climate compared to the rest of the country, as shown in Figures 1(c) and (d), respectively. This is largely the result of topography, with lower temperatures in the highlands than in the rest of the region. The Indian Ocean also influences the hydroclimate of Kenya, with cooler/more humid conditions near the coast and warmer/drier conditions further inland.

The analysis of observed trends in February of daily minimum and daily maximum temperatures (T_{min} and T_{max}, respectively) shows that on average, T_{min} is increasing at 0.6°C per decade since 1995, with eight stations recording a significant positive trend (Figure 1e). Interestingly, the largest T_{min} trends, of ≈1°C dec.$^{-1}$, are located in the highlands. In contrast, T_{max} is stable over the 1995–2024 period, with none of the seven increasing trends nor the three decreasing trends passing the 5% level significance test (Figure 1f).

In this context, we seek to characterise the 15–20 February 2024 event from a climatological perspective, and to gain insights into its meteorological drivers. We focus our

[1] https://www.weather.gov/ama/heatindex.

[2] https://citizen.digital/news/its-unbearable-kenyans-concerned-as-nairobi-gets-too-hot-n336997.

[3] https://theconversation.com/kenyas-had-unusually-hot-weather-an-expert-unpacks-what-could-be-causing-it-224348.

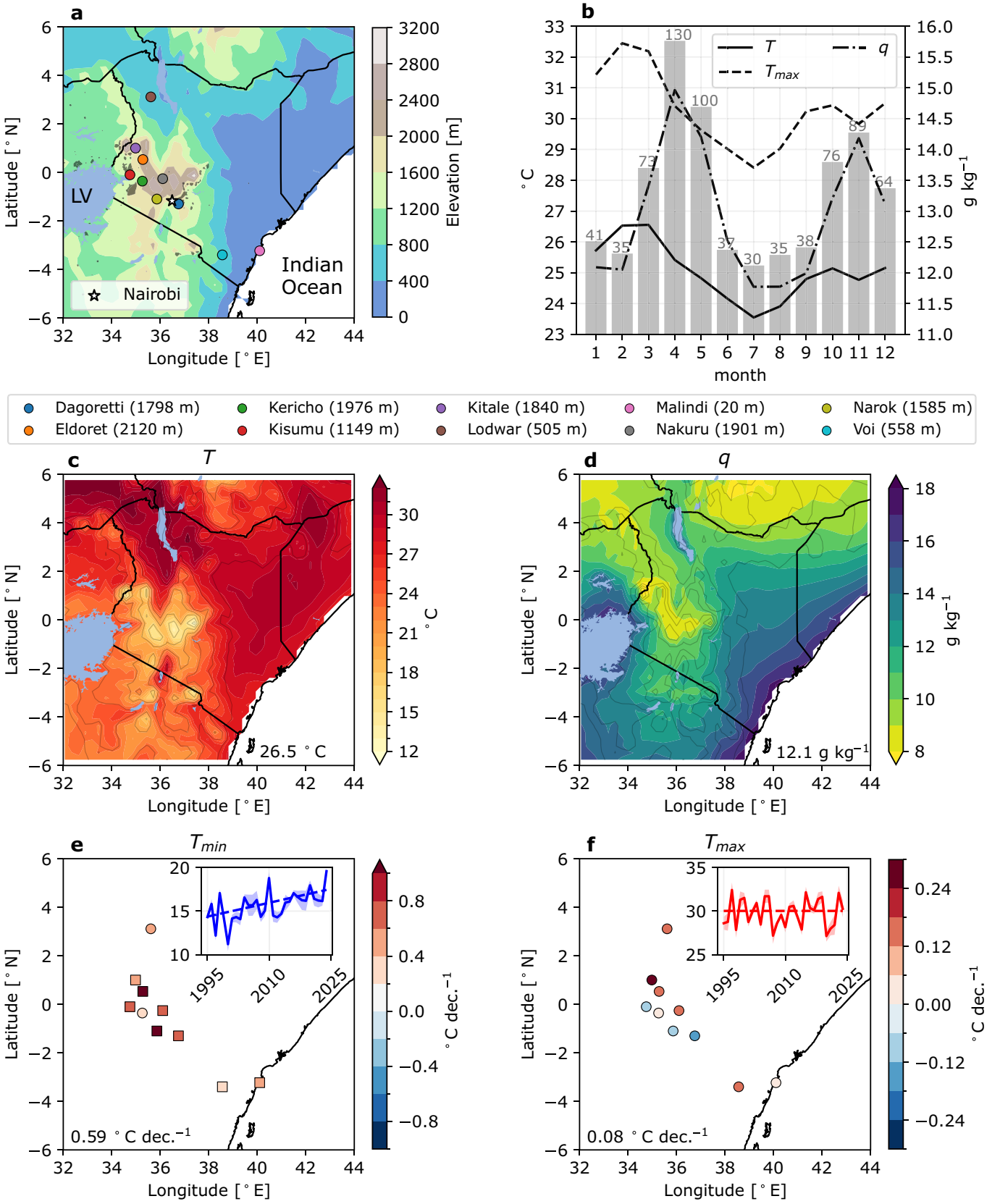

Figure 1. (a) Terrain elevation (shading, in meters) and population density (areas with a population density ≥500 inhabitants km^{-2} are shaded in black). The location of the Kenya Meteorological Department (KMD) stations used in this study are indicated with dots (station names in the legend below). The star denotes Nairobi and 'LV' stands for Lake Victoria. (b) 1995–2024 monthly averages of daily mean temperature (solid line), daily maximum temperature (dashed line), specific humidity (dashed-dotted line), and 2001–2022 mean monthly cumulative rainfall (bars; values indicated on top of each bar, in mm). February mean (c) temperature and (d) specific humidity; the numbers in the bottom right corner of each panel are the spatial averages. Then 1995–2024 trends in February mean (e) T_{min} and (f) T_{max} estimated with a Theil–Sen slope at each KMD station. Trends significant at the 5% level (p-value ≤ 0.05) according to a Mann-Kendall test are depicted with squares. Insets show the time series of regional T_{min} and T_{max} for February. The shading about the lines denotes ±1 standard deviation across stations. The dashed lines are the Theil–Sen trend estimates.

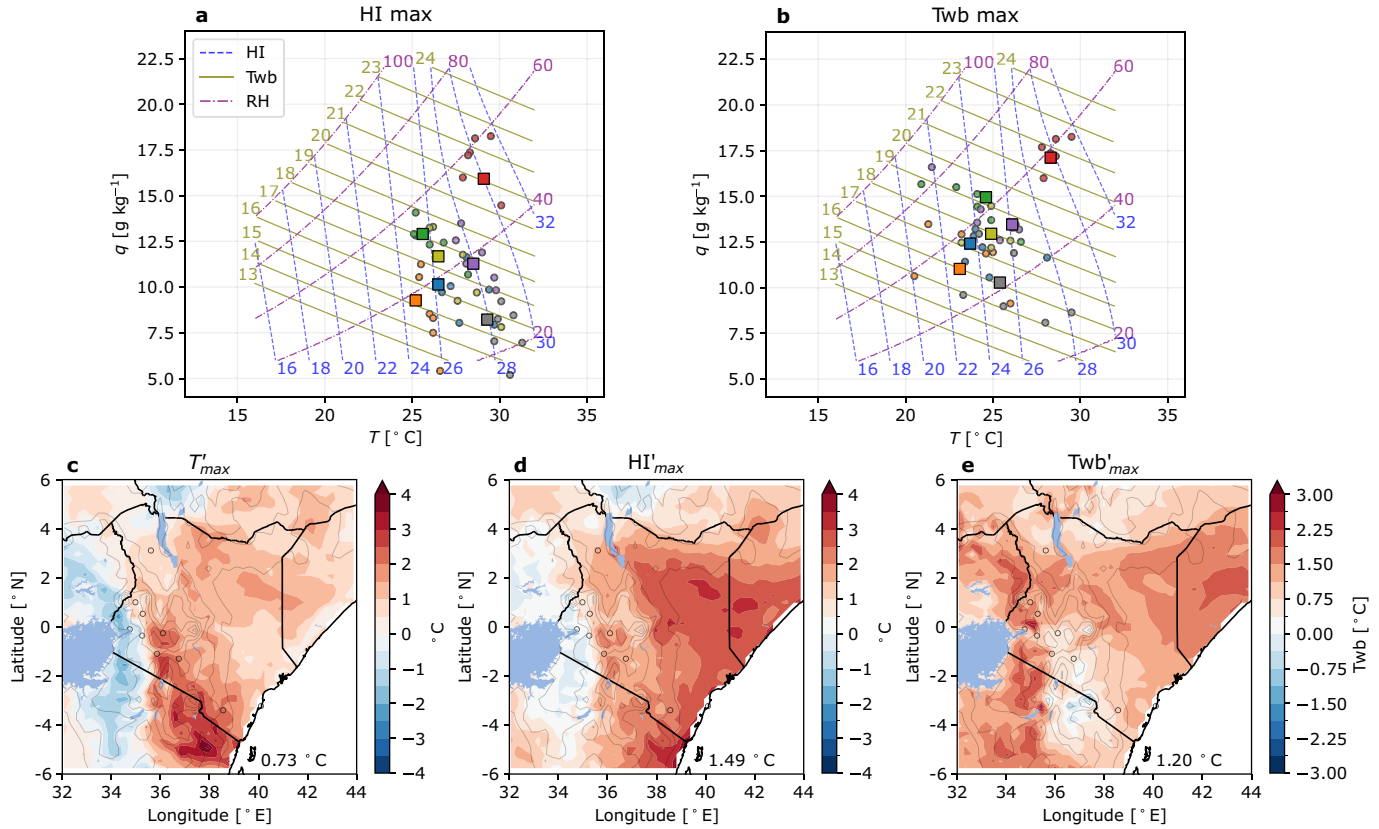

Figure 2. Joint distribution of T *(in °C; x-axis) and* q *(in g kg⁻¹; y-axis) sampled at the time of daily maximum (a) HI and (b) Twb, at each highland station (colour code similar to Figure 1a). Squares denote the median of the marginal distributions of* T *and* q *across all days of February 2024. Dots denote the days between 15 and 20 February 2024. Isolines of HI, Twb and relative humidity (RH) are shown with blue dashed, olive solid and purple dotted-dashed lines, respectively. The 15–20 February 2024 averages in anomalies of daily maximum (c)* T*, (d) HI and (e) Twb (note the different colour scale for this latter). Orography is denoted with grey contours (see Figure 1a for elevation values).*

analysis on the wet-bulb temperature and the Heat Index, whose definitions rely on *T* and *q* only.

Data and methods

Daily rainfall data from the Integrated Multi-satellitE Retrievals for GPM (GPM-IMERG, Huffman *et al*., 2015) for 2001–2022 are used to compute the mean seasonal cycle of rainfall in the study domain (6°S–6°N, 32–44°E). Temperature data extracted from manned weather station records are used to compute trends in monthly means of daily minimum and daily maximum temperatures using a Theil–Sen's slope estimation (Sen, 1968). The significance of trends is assessed with the Mann-Kendall test (Mann, 1945). Hourly dry-bulb temperature, dewpoint temperature and surface pressure provided by automatic weather stations since 2023 are used to compute hourly Twb values with R. Warren and C. Raymond's Python implementation[4] of the Davies-Jones formula (Davies-Jones, 2008). Hourly HI values are calculated from dry-bulb temperature and relative humidity based on the Rothfusz regression (after Steadman, 1979), following the US NWS guidance[5] and with corrections from Romps and Lu (2022). Data from the ERA5 reanalysis (Hersbach *et al*., 2020) are used to compute the regional mean seasonal cycles of daily mean temperature, daily mean specific humidity and daily maximum temperature (Figure 1b). Because the available hourly *in situ* data do not allow for a long-term analysis, ERA5 data are also used to compute daily anomalies in humid heat metrics during 15–20 February 2024 with respect to their 1995–2024 climatology: anomalies of daily maximum *T* (T'_{max}), HI (HI'_{max}), and Twb (Twb'_{max}) are computed separately for each calendar day by subtracting the value for that day to the corresponding 1995–2024 mean, before taking the week average. The significance of the anomalies is assessed with a Mann–Whitney test (Mann and Whitney, 1947).

Results

Figures 2(a) and (b) show, for each highland station, *T* and *q* at the time of daily maxima of HI and Twb, respectively, for each day of 15–20 February 2024 (dots) and averaged across the month (squares). On top of the *T* and *q* values are plotted isolines of HI, Twb and relative humidity (RH). All daily maxima of HI have *T* above 25°C and RH between 20% and 60%. In contrast, observations sampled at the time of daily Twb maxima are associated with cooler and moister (in both absolute and relative terms) environments.

Almost all daily maxima of HI recorded during 15–20 February 2024 are located to the right of the HI isoline that crosses their corresponding monthly mean values (Figure 2a). In contrast, daily maxima of Twb are scattered on either side of the Twb isoline (Figure 2b). Hence, anomalies in humid heat values during 15–20 Febraury 2024 (compared to the month average) were larger for HI than for Twb, meaning that the Heat Index seems more appropriate for assessing the heat stress experienced by the population during this particular episode. It can also be noted in Figures 2(a) and (b) that below about $T = 27$°C, isolines of HI are almost vertical, that is, parallel to isolines of *T*. Therefore, in this region of the $T-q$ space, a departure from the HI climatology is more likely to result from a larger increase in *T* (shift to the right) relative to an increase in *q* (shift upward). In fact, most dots in Figure 2(a) are associated with a clear increase in *T*, whereas changes in *q* have little effect on HI. Beyond these essentially qualitative considerations,

[4]Available at https://github.com/cr2630git/wetbulb_dj08_spedup.

[5]Available at https://www.wpc.ncep.noaa.gov/html/heatindex_equation.shtml.

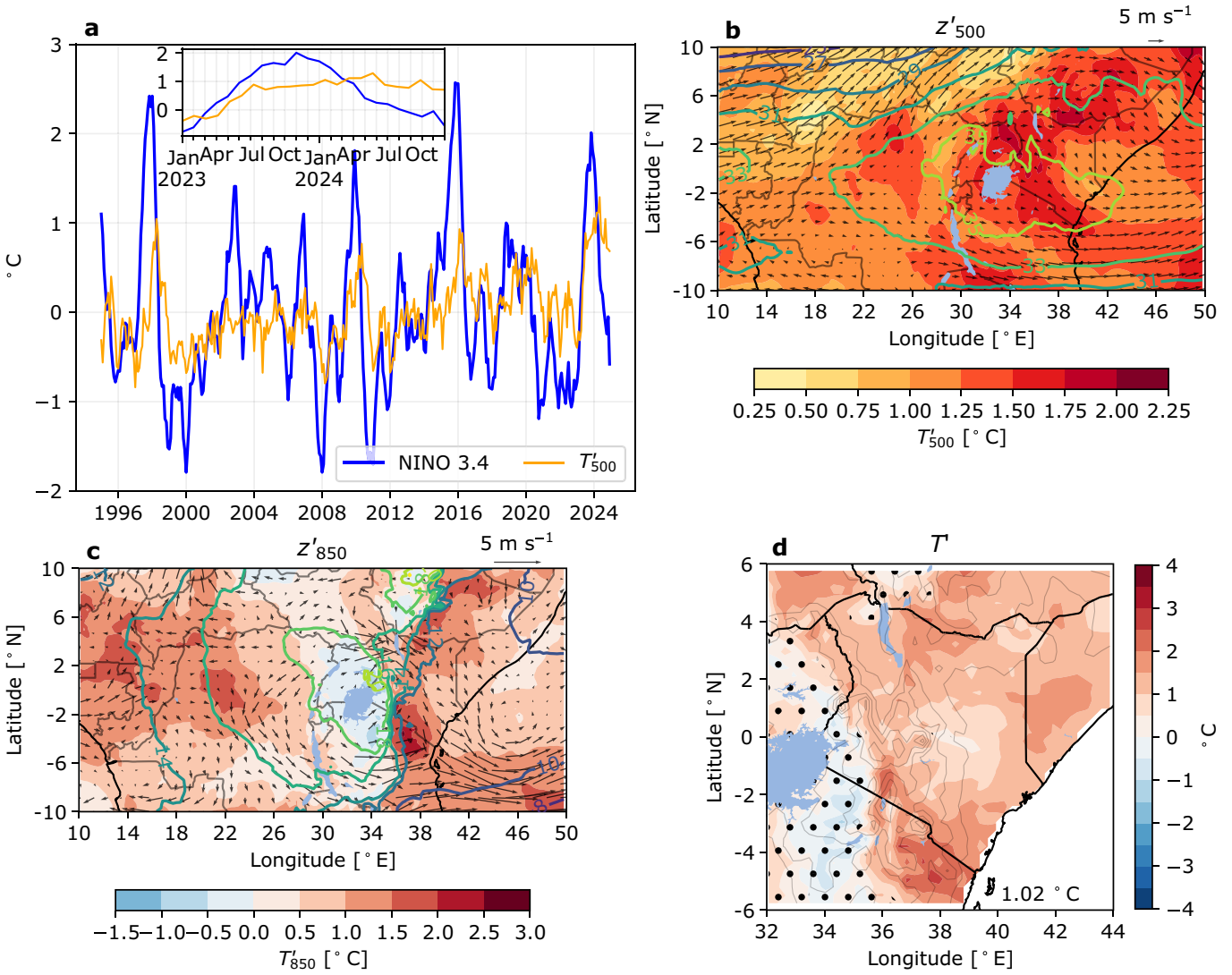

Figure 3. (a) 1995–2024 time series of the monthly El-Nino Southern Oscillation 3.4 index (NINO 3.4, blue line) and the pan-Tropical (30°S–30°N, 180°W–180°E) monthly mean temperature anomaly at 500hPa (T'_{500}, orange line) with respect to the 1995–2024 average. The inset shows the 2023–2024 period. 15–20 February 2024 daily anomaly averages of (b) geopotential height (contours, in m), temperature (shading, in °C) and total wind speed (vectors, in ms^{-1}) at 500hPa. (c) Same as (b) but at 850hPa. (d) 15–20 February 2024 daily anomaly averages of near-surface temperature (T′); the domain-average anomaly is indicated in the bottom right corner; anomalies significant at the 5% level are not stippled; orography is denoted with grey contours (see Figure 1a for elevation values).

it should be noted that several daily maxima of HI recorded during the week belong to the Caution category (HI ∈ [27–32°C]), for which effects on health (e.g. fatigue) begin to occur.

The consequences of heat stress also depend on how unusual it is at a particular time of year and location. We therefore evaluate how daily maxima of *T*, HI and Twb that occurred during 15–20 February 2024 compare with typical values for this time of year (see Data and Methods). Figure 2(c) shows that, on average during the event, T'_{max} is up to 4°C above normal over the eastern highlands. In contrast, negative values are found around Lake Victoria. The HI'_{max} pattern broadly resembles this, with some localised maxima 2–3°C above normal (Figure 2d). The surroundings of Lake Victoria are also cooler than usual, although to a lesser extent than for T'_{max}. Twb'_{max} shows a somewhat opposite pattern, with positive anomalies of 2–3°C in the westernmost part of Kenya and of ≈1°C over the highlands. This confirms that the heat perceived by the population in the highlands was mainly driven by an increase in *T*, with changes in *q* having distinct modulating effects on HI and Twb. We next analyse the meteorological drivers of this event by comparing atmospheric and surface variable values during 15–20 February 2024 with their climatology.

The heat event of February 2024 occurred in the aftermath of the third largest El Nino Southern Oscillation (ENSO) episode since 1995, peaking at +2°C in November 2023 (Figure 3a). ENSO generates warm air temperature anomalies across the Tropics (e.g. Soden, 2000), with tropospheric temperature anomalies generally lagging ENSO by a few months (Sobel *et al.*, 2002, see Figure 3a). Figure 3(b) shows that the mid-troposphere was warmer than usual for this time of year, with air temperature at 500hPa 1.25 to 2.25°C above the long-term average from south-western Kenya to southern Ethiopia. These warm anomalies are associated with a high pressure system centred above Lake Victoria, with 500hPa geopotential height anomalies (z'_{500}) larger than 35m. This high pressure system has a divergent circulation on its northern and southern edges; associated with this, subsidence may have favoured clear-sky conditions and increased solar radiation. A similar situation is seen closer to the surface: air temperature at 850hPa is 1.5 to 3°C above climatology in southern Kenya; the largest geopotential height anomalies, of 10–20m, are centred on Lake Victoria; and there are easterly anomalies of 3–4ms^{-1} on either side of the Lake (Figure 3c). However, air temperature is slightly cooler than usual around Lake Victoria, likely reflecting the influence of surface conditions (due to topography, the 850hPa geopotential height, z_{850}, is close

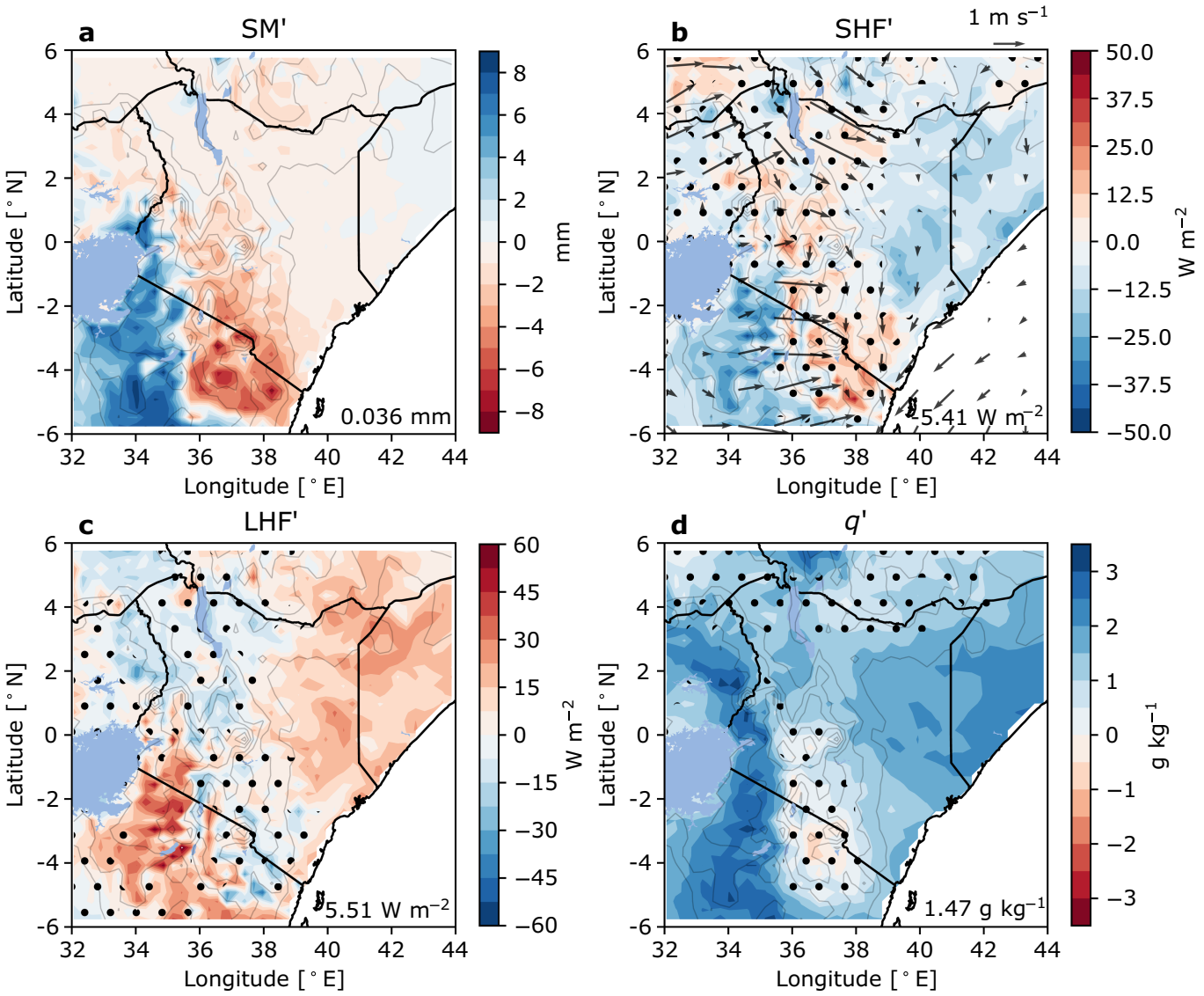

Figure 4. The 15–20 February 2024 daily anomaly averages of (a) top layer soil moisture (SM'), (b) sensible heat flux (SHF'), (c) latent heat flux (LHF'), and (d) specific humidity (q'); 10m wind speed anomalies are also displayed with arrows in (b). The domain-average anomaly for each variable is indicated in the bottom right corner of each panel. Anomalies significant at the 5% level are not stippled, except for SM' where it is the opposite. Orography is denoted with grey contours (see Figure 1a for elevation values).

to the surface in this area). Near-surface air temperature anomalies resemble well their 850hPa counterpart (Figure 3d): T' values of 2–3°C are found in large parts of Kenya, except around Lake Victoria and further South, where T' values of ≈−1°C are found. This confirms that anomalously warm air has contributed substantially to enhancing HI, and to lesser extent Twb (Figures 2d and e, respectively).

We next examine whether the land surface conditions have also played a role in modulating humid heat during the sequence of days. Figure 4(a) shows that top layer (0–7cm) soil moisture anomalies within −2 to −6mm are found over the highlands. Solar radiation hitting drier soils may be preferentially converted into sensible heat flux. Sensible heat flux anomalies of 25–50Wm^{-2}, found in areas of negative soil moisture anomalies (Figure 4b), contribute to enhanced warming of the near-surface air. For reference, a perfectly isolated air volume with a surface of 1×1km and a height of 1km (typically the average depth of the planetary boundary layer) would warm up by ≈0.9°C with a heat flux of 25Wm^{-2} imposed for 12h. Figure 4(a) also shows areas of positive soil moisture anomalies to the East and South of Lake Victoria, resulting in solar radiation being preferentially converted into latent heat flux there, as shown in Figure 4(c). Enhanced evaporation over wet soils moistens the near-surface air, resulting in specific humidity anomalies of 2.5–3.5g kg^{-1} (Figure 4d). These latter explain why positive daily maximum Twb anomalies were found there (Figure 2e), having in mind that Twb is more sensitive to changes in q than to changes in T (Sherwood, 2018).

Discussion and conclusion

This analysis of a heat event from the perspective of two humid heat metrics allows us to infer which metric best captures the heat perceived by the population. It was found that the heat perceived by the inhabitants of the Kenyan highlands during 15–20 February 2024 was largely dry in nature, with daily maxima of dry-bulb temperature 3–4°C above normal, whereas specific humidity was reduced by 0.5–1g kg^{-1}. As a result, daily maxima of the Heat Index were enhanced by 2–3°C, whereas daily maxima of the more q-sensitive wet-bulb temperature were ≈0.5°C below normal for that time of year. In addition, some HI values recorded during the week were close to or within the Caution category, for which health impacts can occur; in contrast, Twb values were below known physiological thresholds. This event resulted from a favourable situation at the synoptic-scale, with mid-tropospheric temperatures 1.25 to 2.25°C above normal following the strong ENSO state that prevailed in the previous months. Furthermore, abnormally high near-surface temperatures were likely amplified by the warming of air

through sensible heat flux enhancement at the expense of surface evaporation over drier soils; this 'upward' land-atmosphere coupling mechanism is known to amplify dry heatwaves (e.g. Seneviratne *et al*., 2006; Miralles *et al*., 2014).

This study contributes to documenting the meteorological drivers of heat hazards in a tropical highland region by considering the modulating and often overlooked role of humidity, and by providing insights on the underlying mechanisms. In this respect, an obvious next step would be to carry out a systematic process-based analysis of dry and humid heat extremes in East Africa, which remains a critical gap in the scientific literature. It should also be noted that Twb and HI may only partially reflect the heat stress experienced by the population, as neither of these metrics considers the role of radiation and wind on human thermoregulation. In fact, anticyclonic conditions are generally associated with clear skies and weak near-surface wind, which would result in larger solar radiation and lower sweat evaporation rates, respectively. It can therefore be expected that heat stress metrics that include one or both variables – such as the wet-bulb globe temperature and the universal thermal comfort index – would display even larger anomalies. On that note, Kong *et al*. (2025) show that inter-metrics spread in heat stress change over the past four decades is primarily driven by differences in temperature-humidity relative weight, suggesting that metrics embedding only these two variables may be sufficient to assess future heat stress trends.

This study was prompted by media reports and is therefore limited in scope. Yet, heat hazards are ubiquitous and their health consequences can remain under the radar, sometimes settling in for the long term (Nunes, 2024). Improving our understanding of the heat–health relationship thus requires systematic surveys that consider the multifaceted effects of heat stress on humans, spanning the diversity of climatological, physiological and socio-economic contexts.

In addition to its effect on health, severe heat can affect a variety of socioeconomic sectors such as agriculture (crops, livestock) and energy (power generation systems). Notwithstanding the fact that quantifying critical thresholds for all the different potential heat impacts remains difficult, these impacts can have high economic costs in sub-Saharan Africa (Burke *et al*., 2015; Parkes *et al*., 2019). Raising awareness and preparing individuals, communities, as well as local and national institutions in sub-Saharan countries, for heat-related risks is therefore crucial under unabated global warming. This study is part of a wider collaboration between the Kenya Meteorological Department and UK-based researchers, aiming at improving heat risk monitoring and forecasting at KMD and across East Africa. KMD has recently implemented humid heat forecasts in their weekly county-level weather bulletins.[6] Future work will be dedicated to the development of an early warning system for heat, combining land surface observations and numerical weather model outputs to predict humid heat hours to days in advance. Heat hazard alerts will be communicated to the last-mile users, including vulnerable populations such as farmers and outdoor workers, via KMD's dissemination channels (SMS, local radio, TV).

Acknowledgements

The authors thank Joshua Talib for initiating this collaboration with KMD and are grateful to KMD staff for the provision and preparation of meteorological data. This work was supported by the Natural Environment Research Council as part of the NC for Global Challenges programme [NE/X006247/1] delivering National Capability.

Author contributions

G. Chagnaud: Conceptualization; data curation; investigation; writing – original draft; writing – review and editing; formal analysis. **J. Gacheru:** Investigation; resources; writing – review and editing; formal analysis. **C. E. Birch:** Funding acquisition; writing – review and editing; validation; investigation. **C. M. Taylor:** Validation; writing – review and editing; funding acquisition; investigation.

Conflict of interest statement

The authors declare no conflict of interest.

Data availability statement

In situ data are the property of the Kenyan Meteorological Department and are not freely available. GPM-IMERG data are available at https://disc.gsfc.nasa.gov/datasets/GPM_3IMERGDF_07/summary. ERA5 data are available from the Copernicus Climate Change Service (C3S) Climate Data Store (CDS) at Hersbach *et al*. (2023). Population density data were extracted from https://www.earthdata.nasa.gov/data/projects/gpw.

References

Baldwin JW, **Benmarhnia T**, **Ebi KL *et al***. 2023. Humidity's role in heat-related health outcomes: a heated debate. *Environ. Health Perspect.* **131**(5): 055001.

Burke M, **Hsiang SM**, **Miguel E**. 2015. Global non-linear effect of temperature on economic production. *Nature* **527**(7577): 235–239.

Buzan JR, **Oleson K**, **Huber M**. 2015. Implementation and comparison of a suite of heat stress metrics within the community land model version 4.5. *Geosci. Model Dev.* **8**(2): 151–170.

Buzan JR, **Huber M**. 2020. Moist heat stress on a hotter Earth. *Annu. Rev. Earth Planet. Sci.* **48**(1): 623–655.

Davies-Jones R. 2008. An efficient and accurate method for computing the wet-bulb temperature along pseudoadiabats. *Mon. Weather Rev.* **136**(7): 2764–2785.

Ebi KL, **Capon A**, **Berry P *et al***. 2021. Hot weather and heat extremes: health risks. *Lancet* **398**(10301): 698–708.

Gasparrini A, **Guo Y**, **Sera F *et al***. 2017. Projections of temperature-related excess mortality under climate change scenarios. *Lancet Planet. Health* **1**(9): e360–e367.

Harrington LJ, **Otto FEL**. 2020. Reconciling theory with the reality of African heatwaves. *Nat. Clim. Chang.* **10**(9): 796–798.

Hersbach H, **Bell B**, **Berrisford P *et al***. 2020. The ERA5 global reanalysis. *Q. J. R. Meteorol. Soc.* **146**(730): 1999–2049.

Hersbach H, **Bell B**, **Berrisford P *et al***. 2023. ERA5 hourly data on single levels from 1940 to present. [Dataset]. Copernicus Climate Change Service (C3S) Climate Data Store (CDS).

Huffman GJ, **Bolvin DT**, **Braithwaite D *et al***. 2015. NASA global precipitation measurement (GPM) integrated multi-satellite retrievals for GPM (IMERG), in Algorithm theoretical basis document (ATBD) version 4.26, pp 30.

Ivanovich CC, **Sobel AH**, **Horton RM *et al***. 2024. Stickiness: a new variable to characterize the temperature and humidity contributions toward humid heat. *J. Atmos. Sci.* **81**(5): 819–837.

Kong Q, **Jing R**, **Raymond C *et al***. 2025. Spatial patterns of historical changes in human heat stress disagree across metrics. *Geophys. Res. Lett.* **52**(20): e2025GL117966.

Luber G, **McGeehin M**. 2008. Climate change and extreme heat events. *Am. J. Prev. Med.* **35**(5): 429–435.

Mann HB, **Whitney DR**. 1947. On a test of whether one of two random variables is stochastically larger than the other. *Ann. Math. Stat.* **18**(1): 50–60.

Mann HB. 1945. Nonparametric tests against trend. *Econometrica* **13**(3): 245–259.

Matthews T, **Raymond C**, **Foster J *et al***. 2025. Mortality impacts of the most extreme heat events. *Nat. Rev. Earth Environ.* **6**(3): 193–210.

Miralles DG, **Teuling AJ**, **Van Heerwaarden CC *et al***. 2014. Megaheatwave temperatures due to combined soil desiccation and atmospheric heat accumulation. *Nat. Geosci.* **7**(5): 345–349.

Nunes AR. 2024. Heatwaves: the silent killers of public health. *Disaster Med. Public Health Prep.* **18**: e227.

Parkes B, **Cronin J**, **Dessens O *et al***. 2019. Climate change in Africa: costs of mitigating heat stress. *Clim. Chang.* **154**(3–4): 461–476.

Perkins SE. 2015. A review on the scientific understanding of heatwaves – their measurement, driving mechanisms, and changes at the global scale. *Atmos. Res.* **164–165**: 242–267.

[6] https://meteo.go.ke/our-products/county-forecasts/.

Romps DM, **Lu Y-C**. 2022. Chronically underestimated: a reassessment of US heat waves using the extended heat index. *Environ. Res. Lett.* **17**(9): 094017.

Schwingshackl C, **Sillmann J**, **Vicedo-Cabrera AM *et al***. 2021. Heat stress indicators in CMIP6: estimating future trends and exceedances of impact-relevant thresholds. *Earth's Future* **9**(3): e2020EF001885.

Sen PK. 1968. Estimates of the regression coefficient based on Kendall's Tau. *J. Am. Stat. Assoc.* **63**(324): 1379–1389. DOI: 10.1080/01621459.1968.10480934

Seneviratne SI, **Lüthi D**, **Litschi M *et al***. 2006. Land–atmosphere coupling and climate change in Europe. *Nature* **443**(7108): 205–209.

Sherwood SC. 2018. How important is humidity in heat stress? *J. Geophys. Res. Atmos.* **123**(21): 11808–11810.

Sherwood SC, **Huber M**. 2010. An adaptability limit to climate change due to heat stress. *Proc. Natl. Acad. Sci. USA* **107**(21): 9552–9555.

Simpson CH, **Brousse O**, **Ebi KL *et al***. 2023. Commonly used indices disagree about the effect of moisture on heat stress. *NPJ Clim. Atmos. Sci.* **6**(1): 78.

Sobel AH, **Held IM**, **Bretherton CS**. 2002. The ENSO signal in tropical tropospheric temperature. *J. Clim.* **15**(18): 2702–2706.

Soden BJ. 2000. The sensitivity of the tropical hydrological cycle to ENSO. *J. Clim.* **13**(3): 538–549.

Steadman RG. 1979. The assessment of sultriness. Part I: a temperature-humidity index based on human physiology and clothing science. *J. Appl. Meteorol. Climatol.* **18**(7): 861–873.

Vanos J, **Guzman-Echavarria G**, **Baldwin JW *et al***. 2023. A physiological approach for assessing human survivability and liveability to heat in a changing climate. *Nat. Commun.* **14**(1): 7653.

Vecellio DJ, **Wolf ST**, **Cottle RM *et al***. 2022. Evaluating the 35°C wet-bulb temperature adaptability threshold for young, healthy subjects (PSU HEAT project). *J. Appl. Physiol.* **132**(2): 340–345.

Vicedo-Cabrera AM, **Scovronick N**, **Sera F *et al***. 2021. The burden of heat-related mortality attributable to recent human-induced climate change. *Nat. Clim. Chang.* **11**(6): 492–500.

Correspondence to: G. Chagnaud
guicha@ceh.ac.uk

doi: 10.1002/wea.70011